Cellular/Molecular

The *FGF14*^{F145S} Mutation Disrupts the Interaction of FGF14 with Voltage-Gated Na$^+$ Channels and Impairs Neuronal Excitability

Fernanda Laezza,[1,2] **Benjamin R. Gerber,**[1] **Jun-Yang Lou,**[1] **Marie A. Kozel,**[1] **Hali Hartman,**[3] **Ann Marie Craig,**[2] **David M. Ornitz,**[1] **and Jeanne M. Nerbonne**[1]

Departments of [1]Molecular Biology and Pharmacology and [2]Anatomy and Neurobiology, Washington University Medical School, St. Louis, Missouri 63110, and [3]Institute of Molecular Cardiology, University of Maryland Biotechnology Institute, Baltimore, Maryland 21201

Fibroblast growth factor 14 (FGF14) belongs to the intracellular FGF homologous factor subfamily of FGF proteins (iFGFs) that are not secreted and do not activate tyrosine kinase receptors. The iFGFs, however, have been shown to interact with the pore-forming (α) subunits of voltage-gated Na$^+$ (Na_v) channels. The neurological phenotypes seen in *Fgf14*$^{-/-}$ mice and the identification of an *FGF14* missense mutation (*FGF14*^{F145S}) in a Dutch family presenting with cognitive impairment and spinocerebellar ataxia suggest links between FGF14 and neuronal functioning. Here, we demonstrate that the expression of FGF14^{F145S} reduces Na_v α subunit expression at the axon initial segment, attenuates Na_v channel currents, and reduces the excitability of hippocampal neurons. In addition, and in contrast with wild-type FGF14, FGF14^{F145S} does not interact directly with Na_v channel α subunits. Rather, FGF14^{F145S} associates with wild-type FGF14 and disrupts the interaction between wild-type FGF14 and Na_v α subunits, suggesting that the mutant FGF14^{F145S} protein acts as a dominant negative, interfering with the interaction between wild-type FGF14 and Na_v channel α subunits and altering neuronal excitability.

Key words: **FHFs; Na_v channels; action potentials; repetitive firing; axon initial segment; α subunit**

Introduction

Fibroblast growth factor 14 (FGF14) belongs to the intracellular FGF homologous factor family (iFGFs), a distinct set of four neuronally expressed FGFs (iFGF11–14) that are not secreted and do not activate tyrosine kinase receptors (Ornitz and Itoh, 2001; Olsen et al., 2003; Itoh and Ornitz, 2004; Goldfarb, 2005). A missense mutation in the *FGF14* gene, *FGF14*^{F145S}, was identified in a Dutch family presenting with multiple neurological deficits including impaired cognitive abilities and spinocerebellar ataxia (Van Swieten et al., 2003), and is now classified as spinocerebellar ataxia 27 [OMIM (Online Mendelian Inheritance in Man) number 609307, SCA27].

The spectrum of neurological phenotypes evident in SCA27 individuals suggests that FGF14 is important for the normal functioning of multiple areas of the central, and possibly the peripheral, nervous system (Manto, 2005). Consistent with this suggestion, genetic ablation of *Fgf14* in mice (*Fgf14*$^{-/-}$) results in ataxia, paroxysmal dystonia (Wang et al., 2002), and cognitive impairment (Wozniak et al., 2007). Protein modeling studies suggest that the phenylalanine (F) to serine (S) mutation at residue 145 reduces FGF14 stability, resulting in loss of FGF14 function (Olsen et al., 2003; Van Swieten et al., 2003). The autosomal-dominant nature of the *FGF14*^{F145S} mutation and the similarity between the phenotypes of SCA27 patients and *Fgf14*$^{-/-}$ mice further suggests that the *FGF14*^{F145S} mutation results in a loss of FGF14 function.

In the hippocampus, *Fgf14* is expressed in pyramidal neurons and in the dentate gyrus (Smallwood et al., 1996; Wang et al., 2002; Lou et al., 2005; Xiao et al., 2007), and loss of FGF14 in *Fgf14*$^{-/-}$ mice results in impaired long-term potentiation at Schaffer collaterals–CA1 synapses (Xiao et al., 2007). It has been demonstrated that the iFGFs interact directly with the pore-forming (α) subunits of neuronal and cardiac voltage-gated Na$^+$ (Na_v) channels and heterologous coexpression of FGF12, FGF13, or FGF14 with Na_v α subunits differentially affects Na_v current densities and the voltage dependences of Na_v channel activation and inactivation (Liu et al., 2001, 2003; Wittmack et al., 2004; Lou et al., 2005; Rush et al., 2006). In rat hippocampal neurons, heterologously expressed FGF14 colocalizes with native Na_v channels at the axon initial segment (AIS) (Lou et al., 2005), a specialized subcellular domain of high-Na_v channel density that

Received May 18, 2007; revised Sept. 10, 2007; accepted Sept. 16, 2007.

This work was supported by Washington University, National Institutes of Health Grant NS030676 (J.M.N.), and the McDonnell Center for Cellular and Molecular Neurobiology (D.M.O. and J.M.N.). J.-Y.L. was supported by Cardiovascular Pharmacology Training Grant T32-HL07275 and the Medical Scientist Training Program, Washington University. We thank Dr. M. Komada (Tokyo Institute of Technology, Tokyo, Japan) for providing the affinity-purified chicken anti-βIV-spectrin antibody and Dr. C. Mulle (University of Bordeaux, Bordeaux, France) for providing the *myc-GluR6* construct. In addition, we thank Dr. T. K. Pilgram for advice on statistical analyses and H. Wu and L. Li for technical assistance in the preparation and maintenance of hippocampal cultures.

Correspondence should be addressed to Dr. Jeanne M. Nerbonne, Department of Molecular Biology and Pharmacology, Box 8103, Washington University Medical School, 660 South Euclid Avenue, St. Louis, MO 63110. E-mail: jnerbonne@wustl.edu.

A. M. Craig's present address: Brain Research Centre, University of British Columbia, 2211 Wesbrook Mall, Vancouver, British Columbia, Canada V6T 2B5.

DOI:10.1523/JNEUROSCI.2282-07.2007

 0270-6474/07/2712033-12$15.00/0

regulates action potential initiation and propagation (Clark et al., 2005; Meeks et al., 2005; Khaliq and Raman, 2006; Van Wart et al., 2007).

Alterations in Na_v channel expression or function will impact neuronal membrane excitability and information processing in neuronal circuits. Indeed, mutations in genes encoding Na_v channel subunits (Bechtold and Smith, 2005; Meisler and Kearney, 2005) or alterations in the expression of proteins necessary for the localization of Na_v channels at the AIS (Garrido et al., 2003b) dramatically affect the output properties of central neurons. Together, these observations suggest that $FGF14^{F145S}$ expression might affect neuronal excitability by interfering with the functioning of Na_v channels. The experiments here were designed to test this hypothesis and to explore the mechanism(s) underlying the functional effects of $FGF14^{F145S}$.

Materials and Methods

Plasmids. The *Fgf14-Gfp* (*Fgf14-1b-Gfp*), *Fgf14-myc* (*Fgf14-1b-myc*), and *hSpry-Myc* fusion constructs were generated and characterized as described previously (Lou et al., 2005). The F145S mutation in *Fgf14* was introduced into the *Fgf14-Gfp* and *Fgf14-myc* constructs and verified by sequencing. The numbering used for the FGF14 protein sequence is based on the numbering system for human FGF14-1a (Van Swieten et al., 2003). The *myc-GluR6* construct (Coussen et al., 2002) was a gift from Dr. C. Mulle (University of Bordeaux, Bordeaux, France).

Cell culture and transient transfections. All reagents were purchased from Sigma (St. Louis, MO) unless noted otherwise. HEK-293 cells stably expressing rat $Na_v1.2$ (HEK-Nav1.2 cells) were maintained in DMEM (Invitrogen, Carlsbad, CA); supplemented with 10% fetal bovine serum, 100 U/ml penicillin, 100 μg/ml streptomycin, and 500 μg/ml G418 (Invitrogen); and incubated at 37°C with 5% CO_2. Cells were transfected at 90–100% confluency using Lipofectamine 2000 (Invitrogen), according to manufacturer's instructions.

Hippocampal cultures were prepared from embryonic day 18 rat embryos using previously described methods (Goslin et al., 1998). Briefly, hippocampi were dissected and dissociated using trypsin and trituration through a Pasteur pipette. Neurons were plated at low density ($1–5 \times 10^5$ cells per dish) on poly-L-lysine-coated coverslips in 60 mm culture dishes in MEM supplemented with 10% horse serum. After 2–4 h, coverslips (containing neurons) were inverted and placed over a glial feeder layer in serum-free MEM with 0.1% ovalbumin and 1 mM pyruvate (N2.1 medium; Invitrogen) separated by ~1 mm wax dot spacers. The presence of the spacer prevented contact between the neurons on the coverslips and the glial feeder layer. Cultures were maintained in N2.1 medium in the presence of 100 μM D,L-2-amino-5-phosphonovaleric acid (APV; Research Biochemicals, Natick, MA), to prevent glutamate excitotoxicity, for up to 10 d. To prevent the overgrowth of the glia, cultures were treated with cytosine arabinoside (5 μM; Calbiochem, La Jolla, CA) at 3 d *in vitro* (DIV). Transfections were performed using Lipofectamine 2000 (Invitrogen) at 9 DIV for imaging and current-clamp recordings and at 0 DIV for voltage-clamp recordings.

Immunofluorescence. Rat hippocampal neurons (10 or 14 DIV) were fixed in fresh 4% paraformaldehyde and 4% sucrose in PBS for 15 min and permeabilized with 0.25% Triton X-100. After blocking with 10% BSA for ~30 min at 37°C, neurons were incubated at room temperature for 12–16 h with one of the following combinations of primary antibodies: mouse monoclonal anti-Pan Na_v α subunit (diluted 1:100; Sigma) and rabbit polyclonal anti-microtubule-associated protein 2 (MAP2; diluted 1:1000; Chemicon, Temecula, CA); or mouse monoclonal anti-FGF14 (diluted 1:1000; Antibodies, Davis, CA) and chicken polyclonal anti-βIV-spectrin (diluted 1:2000). The FGF14 monoclonal antibody was developed against a GST-FGF14-1b fusion protein (pET-42-GST-FGF14-1b) and affinity purified. The affinity-purified chicken anti-βIV-spectrin antibody (Komada and Soriano, 2002; Nishimura et al., 2007) was generously provided to us by Dr. M. Komada (Tokyo Institute of Technology, Tokyo, Japan). All antibodies were diluted (as the concentrations noted) in PBS containing 3% BSA.

After incubations with the primary antibody combinations, neurons were washed three times in PBS and incubated for 2 h at 37°C with appropriate secondary antibodies: Alexa 647-conjugated goat anti-mouse IgG_1 (1:500) together with aminomethylcoumarin (AMCA)-conjugated goat anti-rabbit IgG (1:100; Vector Laboratories, Burlingame, CA) for the cells stained with the mouse monoclonal anti-Pan Na_v α subunit and the rabbit polyclonal anti-MAP2 antibodies; or Alexa 568-conjugated goat anti-mouse IgG and Alexa 488-conjugated goat anti-chicken IgY for the cells stained with the mouse monoclonal anti-FGF14 and chicken polyclonal anti-βIV-spectrin antibodies. Coverslips were then washed (three times) with PBS and mounted in elvanol (Tris-HCl, glycerol, and polyvinyl alcohol with 2% 1,4-diazabicyclo[2,2,2] octane) or in Prolong Gold anti-fade reagent (Invitrogen). Images were acquired using an Axoplan 2 or Axio Imager epifluorescence microscope (Zeiss, Oberkochen, Germany) with a 63× objective. Images were acquired with a CCD camera using MetaMorph (Universal Imaging, Downingtown, PA) or with an Axio Cam MRm using the Axio Vision software (Zeiss).

Image quantification. For pixel intensity quantification, image files from each group, from two independent sets of transfections, were acquired blindly. Images were saved as TIFF files and analyzed with MetaMorph (Universal Imaging). On each cell analyzed, a line, 3 pixels in width and 20 μm in length, was drawn down the axon on an overlay image of the monomeric red fluorescent protein (mRFP) or green fluorescent protein (GFP) and MAP2 staining. This line was then transferred to the Alexa 647 image, which reflected the Na_v α subunit labeling. In each cell, the axon was unequivocally identified as a thin process, positive for mRFP or GFP and negative for MAP2. The "starting point" for length measurements was the point of reduced MAP2 staining intensity; this proved to be a reliable marker of increased Na_v channel density, corresponding to the AIS, in GFP-expressing (control) neurons. To adjust for uneven illumination, images were processed for flat-field correction, before analysis. The intensity of off-cell background fluorescence was numerically subtracted at the end of the line-scan analysis. Total fluorescence intensity of immunolabeled Na_v channels at the AIS was measured from cells in each experimental group. To combine data from independent sets of transfections, total fluorescence intensity values were normalized to the mean value of the GFP control of that set. Intensity profiles of individual and average traces for each experimental group were generated by plotting pixel intensity values along distance. Data were tabulated and analyzed with Excel, Origin, and SigmaStat (Jendel Corporation, San Rafael, CA).

Immunoprecipitations. HEK-293 cells, stably expressing the rat $Na_v1.2$ α subunit, were washed twice with PBS and lysed in the following lysis buffer: 20 mM Tris-HCl, 150 mM NaCl, and 1% NP-40 or Triton X-100. Protease inhibitor mixture (Cocktail #3; Calbiochem) was added immediately before cell lysis. Cell extracts were collected and sonicated for 20 s and centrifuged at 4°C, at 15,000 × *g* for 15 min. Supernatants were collected and incubated with rabbit anti-myc agarose beads (Sigma) for 2 h at 4°C with agitation. After washing five times with lysis buffer, 2× sample buffer (Bio-Rad, Hercules, CA) containing 50 mM TCEP [tris(2-carboxyethyl) phosphine] was added. Lysates were then heated for 10–15 min at 65°C and resolved on 7.5% or 4–15% polyacrylamide gradient gels (Bio-Rad). Resolved proteins were transferred to polyvinylidene difluoride membranes (Millipore, Bedford, MA) for 2 h at 4°C and blocked in Tris-buffered saline with 5% skim milk and 0.1% Tween 20. Membranes were then incubated in blocking buffer containing a monoclonal anti-myc (1:1000; Santa Cruz Biotechnology, Santa Cruz, CA) or anti-PanNa_v channel (1:1000; Sigma) antibody overnight at 4°C. Washed membranes were incubated with goat anti-mouse HRP (1:5000–10,000) detected with SuperSignal Fempto chemiluminescent substrate (Pierce, Rockford, IL). Signals were revealed either with Kodak (Rochester, NY) BioMax films or with Chemidoc XRS (Bio-Rad). Data were analyzed using Quantity One software (Bio-Rad).

Electrophysiology. Recordings were obtained from rat hippocampal neurons isolated at 1 DIV (for voltage-clamp recordings) or 10 DIV (for current-clamp recordings) at room temperature (20–22°C) ~12–18 h after transfection using a Dagan Corporation (Minneapolis, MN) model 3900 amplifier. Borosilicate glass pipettes were fabricated using a P-87

micropipette puller (Sutter Instruments, Novato, CA); tip resistances were 2.5–5 MΩ. For voltage-clamp recordings, the extracellular bath solution contained (in mM) 140 NaCl, 3 KCl, 1 $MgCl_2$, 1 $CaCl_2$, and 20 HEPES, pH 7.3; the bath solution also contained bicuculline (10 μM), CNQX (6-cyano-7-nitroquinoxaline-2,3-dione; 30 μM), and APV (100 μM) to block synaptic activity mediated by GABA, AMPA, and NMDA receptors, respectively. Recording pipettes contained (in mM) 140 CsF, 1 EGTA, 10 NaCl, and 10 HEPES, pH 7.3. For current-clamp recordings, the extracellular bath solution contained (in mM) 140 NaCl, 4 KCl, 10 HEPES, 10 glucose, 2 $MgCl_2$, and 2 $CaCl_2$, pH 7.3, and the intracellular recording solution contained (in mM) 130 KCl, 10 HEPES, 10 glucose, 1.1 $CaCl_2$, 2.6 BAPTA, 3 MgATP, and 0.5 NaGTP, pH 7.3.

After seal formation and membrane rupture, whole-cell membrane currents, evoked in response to brief (5 ms) hyperpolarizing voltage steps to −80 mV from a holding potential of −70 mV, were recorded. Input resistances, series resistances, and whole-cell capacitances were derived from these uncompensated current records. Capacitative transients and series resistances were then compensated electronically (by ~80–90%) before recording voltage-gated currents. Data were acquired at 50 kHz and filtered at 5 kHz before digitization and storage. All experimental parameters were controlled using the Clampex 9.2 software (Molecular Devices, Union City, CA), interfaced to the electrophysiological equipment using a Digidata 1322A analog-to-digital interface (Molecular Devices). Voltage-dependent inward Na^+ (Na_v) currents were evoked by brief (50–100 ms) depolarizing voltage steps to test potentials between −60 and +60 mV from a holding potential of −90 mV. For measurement of steady-state inactivation, cells were stepped to varying conditioning potentials between −130 and −20 mV for 750 ms (from a holding potential of −90 mV) before the test depolarizations to −10 mV (to measure the amplitude of the Na_v currents).

Single action potentials and action potential trains were recorded in response to brief (2 ms) and prolonged (0.5–1 s), respectively, depolarizing current injections of variable amplitudes. To determine the effects of suppression of Na_v currents on action potential waveforms in hippocampal neurons, cells were exposed to brief applications of 1–10 nM tetrodotoxin (TTX), delivered locally from a micropipette using a gravity-based perfusion system.

Data analysis. Analysis of electrophysiological data were performed using Clampfit 9.2 (Molecular Devices), Origin 6.1 (OriginLab Corporation, Northampton, MA), and Prizm 4 (Graph Pad, San Diego, CA). Peak Na_v current densities were obtained by dividing peak Na_v current amplitudes in each cell by the whole-cell membrane capacitance (measured in the same cell), and the Na_v conductance (at each test potential and in each cell), G_{Na}, was calculated using the following equation:

$$G_{Na} = I_{Na}/(V_m - E_{rev}),$$

where I_{Na} is the current amplitude at voltage V_m and E_{rev} is the calculated Na^+ reversal potential. Normalized conductances were then calculated as $G_{Na}/G_{Na,Max}$, where $G_{Na,Max}$ is the maximal conductance. Steady-state activation curves were derived by plotting the normalized G_{Na} ($G_{Na}/G_{Na,Max}$) as a function of test potential and fitted using a Boltzman equation of the following form:

$$G_{Na}/G_{Na,Max} = 1 + e^{[(Va - Vm)/k]},$$

where V_a is the membrane potential of half-maximal activation and k is the slope factor.

For steady-state inactivation, normalized current amplitudes ($I_{Na}/I_{Na,Max}$) at each test potential in each cell were determined, and mean values were plotted as a function of prepulse potential (V_m) and fitted using a Boltzman equation of the following form:

$$I_{Na}/I_{Na,Max} = 1/[1 + e^{[(Vh - Vm)/k]}],$$

where V_h is the voltage of half-maximal inactivation and k is the slope factor.

Statistical analysis. All the results are presented as means ± SEM. The statistical significance of differences between groups was assessed using either a parametric t test or nonparametric t test, based on the distribution of the samples underlying the populations, and was set at $p < 0.05$. Statistical analysis was performed using SigmaStat (Jendel Corporation).

Results

Expression of FGF14^{F145S} disrupts localization of Na_v channels at the AIS

To explore directly the effects of FGF14^{F145S} on the distribution and localization of neuronal Na_v channels, rat hippocampal neurons were cotransfected with cDNA constructs encoding mRFP (*mRfp*) and GFP-tagged FGF14^{F145S} (*Fgf14^{F145S}-Gfp*). Parallel experiments were conducted on cells cotransfected with constructs encoding *mRfp* and either an epitope (GFP)-tagged wild-type *Fgf14-1b* (*Fgf14-Gfp*) or *Gfp* alone. Approximately 24 h after transfection, cells were fixed and stained with a monoclonal anti-Pan Na_v α subunit-specific antibody and with a polyclonal antibody against the MAP2, a commonly used somato-dendritic marker (Garrido et al., 2003b; Fache et al., 2004). In neurons transfected with the *Gfp* construct (Fig. 1*A–F*), robust Na_v channel expression was evident in the proximal regions of thin MAP2-negative processes (Fig. 1*B*,*C*,*F*), corresponding to the AIS (Garrido et al., 2003a; Van Wart et al., 2007). In contrast, in neurons expressing FGF14^{F145S}-GFP (Fig. 1*G–L*), Na_v channel labeling in the AIS was markedly reduced (Fig. 1*H*,*L*), whereas in hippocampal neurons expressing (wild-type) FGF14-GFP (Lou et al., 2005) (Fig. 1*M–R*), Na_v channel labeling in the AIS was increased (Fig. 1*N*,*R*).

For quantification of Na_v α subunit expression, line-scan analyses of fluorescence intensities along the AIS region in individual hippocampal neurons (Fig. 1*S–U*) were performed. These analyses revealed that the total fluorescence intensity of immunolabeled Na_v channels was markedly reduced (by ~50%) in neurons expressing FGF14^{F145S} (Fig. 1*T*) compared with cells expressing GFP (Fig. 1*S*) or FGF14-GFP (Fig. 1*U*). The mean ± SEM Na_v α subunit labeling intensity along the AIS in neurons expressing FGF14^{F145S} ($n = 47$) was 54 ± 6% of the (mean ± SEM) intensity in GFP-expressing cells, a value that is significantly ($p < 0.001$) lower than in cells expressing GFP ($n = 40$) or FGF14-GFP ($n = 58$) (Fig. 1*V*). Average Na_v α subunit labeling intensity in the AIS was also significantly ($^{\ddagger}p < 0.05$) higher in FGF14-GFP-expressing, compared with GFP-expressing (Fig. 1*V*) cells. In addition, although detectable in the MAP2-positive somato-dendritic compartments of hippocampal neurons, FGF14^{F145S} was barely or not detectable in axons and was not enriched at the AIS (Fig. 1*G*). Thus, in contrast to wild-type FGF14 (Fig. 1*M*,*N*), FGF14^{F145S} does not colocalize in hippocampal neurons with native Na_v channel α subunits at the AIS (Fig. 1*G*,*H*).

Expression of FGF14^{F145S} suppresses peak Na_v current densities in hippocampal neurons

It has previously been demonstrated that overexpression of FGF14-GFP in isolated rat hippocampal neurons modulates Na_v channel currents (I_{Na}), increasing peak current densities and shifting the voltage dependences of current activation and inactivation (Lou et al., 2005). To determine directly the effects of FGF14^{F145S} on endogenous neuronal Na_v current densities and properties, whole-cell voltage-clamp recordings were obtained from hippocampal neurons 12–24 h after transfection with *Fgf14^{F145S}-Gfp*, *Fgf14-Gfp*, or *Gfp*. Recordings were obtained from cells lacking extensive neurites to ensure adequate voltage-clamp control. Representative recordings from GFP-, FGF14^{F145S}-GFP-, and FGF14-GFP-expressing cells are illustrated in Figure 2*A–C*. Robust, rapidly activating Na_v currents

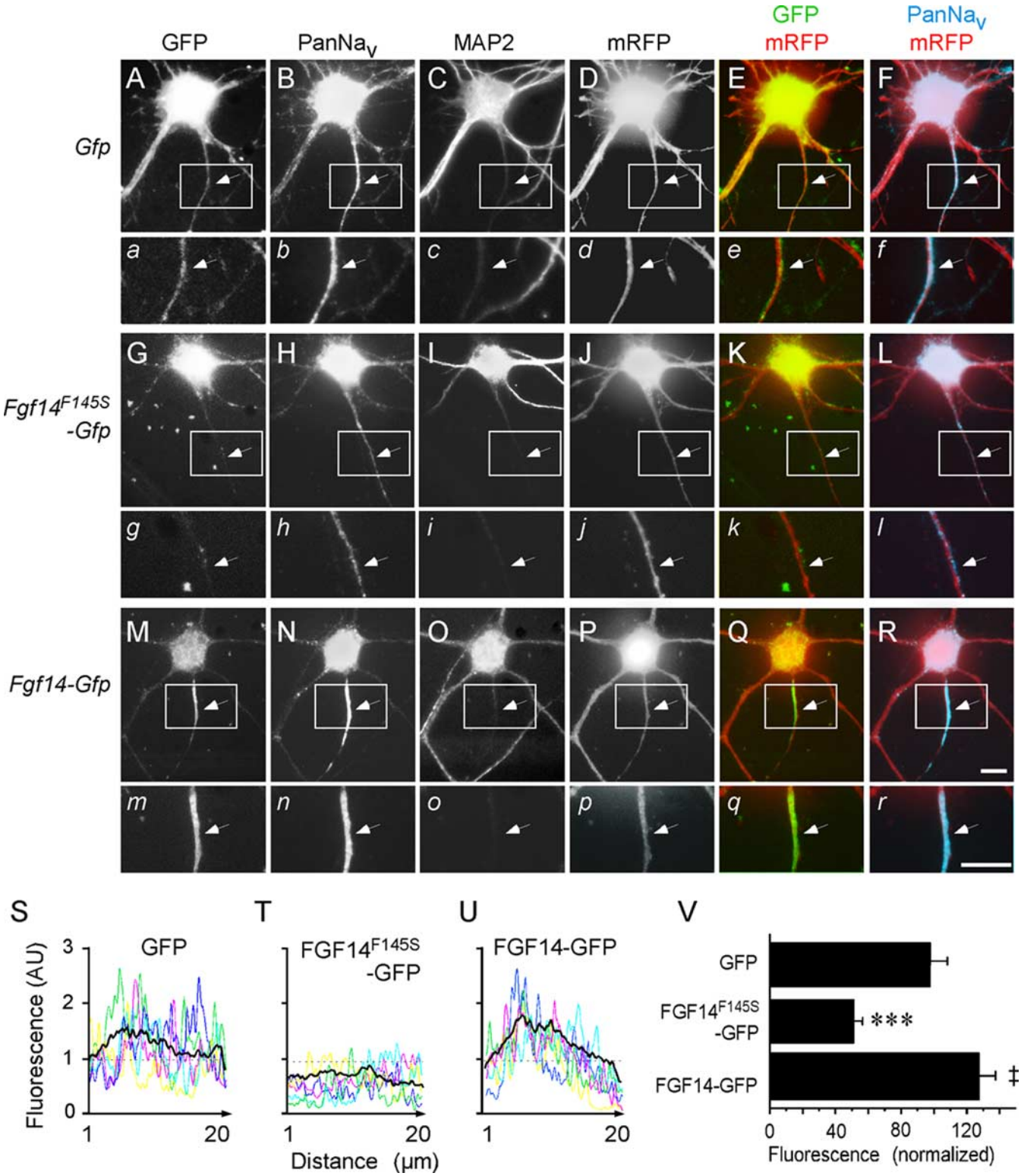

Figure 1. Na_v channel localization at the AIS is disrupted by expression of $FGF14^{F145S}$. ***A–R***, Fluorescence images of rat hippocampal neurons expressing mRFP together with GFP (***A–F***), $FGF14^{F145S}$-GFP (***G–L***), or FGF14-GFP (***M–R***) stained with a monoclonal anti-Na_v α subunit-specific antibody, $PanNa_v$, visualized with an Alexa 647-conjugated secondary antibody (***B***, ***H***, ***N***), and a polyclonal anti-MAP2 antibody, visualized with an AMCA-conjugated secondary antibody (***C***, ***I***, ***O***). GFP fluorescence images are shown in ***A***, ***G***, and ***M***, and mRFP fluorescence images are shown in ***D***, ***J***, and ***P***. Overlay images of GFP and mRFP are shown in the green and red channels (***E***, ***K***, ***Q***). Overlay images of $PanNa_v$ and mRFP are shown in cyan and red channels (***F***, ***L***, ***R***). The bottom panels (***a–r***) are high-magnification images of the boxed regions in each of the corresponding panels ***A–R***, presented to highlight the AIS regions (arrows). Comparing ***B***, ***H***, and ***N***, it is evident that the intensity of the Na_v α subunit labeling in the AIS regions is lower in the $FGF14^{F145S}$-expressing neuron (***H***) and is higher in the FGF14-expressing neuron (***N***) than in the cell expressing GFP (***B***). Scale bars, 10 μm. ***S–U***, Representative examples of Na_v α subunit immunofluorescence intensity line scans along the AIS regions in individual neurons expressing GFP (***S***), $FGF14^{F145S}$-GFP (***T***), or FGF14-GFP (***U***). In each panel, the black line indicates the mean fluorescence intensity profile obtained from GFP-expressing (***S***; $n = 20$), $FGF14^{F145S}$-GFP-expressing (***T***; $n = 23$), or FGF14-GFP-expressing (***U***; $n = 28$) neurons from one set of transfections. ***V***, Mean $\pm$ SEM of Na_v α subunit immunofluorescence intensities in GFP-expressing ($n = 40$), $FGF14^{F145S}$-GFP-expressing ($n = 47$), and FGF14-GFP-expressing ($n = 58$) cells are plotted. Values were normalized to the mean control value determined in GFP-expressing cells ($^{‡}p < 0.05$; $^{***}p < 0.001$).

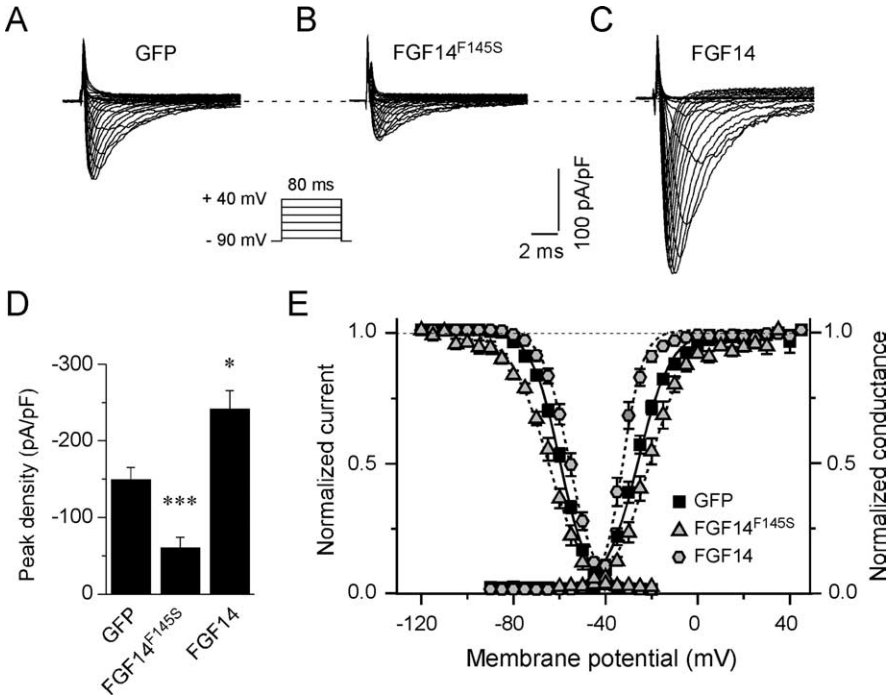

Figure 2. Expression of FGF14F145S attenuates peak Nav current densities in hippocampal neurons. ***A–C***, Representative whole-cell voltage-gated inward Na^+ (Na_v) currents recorded from isolated hippocampal neurons in response to depolarizing voltage steps to potentials ranging from −60 to +40 mV from a holding potential of −90 mV as described in Materials and Methods. The voltage-clamp protocol is illustrated below the current records. ***D***, Mean ± SEM peak Na_v current densities in hippocampal neurons expressing $FGF14^{F145S}$-GFP ($n = 29$) are significantly (***$p < 0.001$) lower than in cells expressing GFP ($n = 38$), whereas mean ± SEM peak Na_v current densities in FGF14-GFP ($n = 17$)-expressing cells are significantly (*$p < 0.01$) higher. ***E***, Small but statistically significant (**$p < 0.005$) differences in the voltage dependences of Na_v channel activation and inactivation are evident in cells overexpressing FGF14 and in cells expressing $FGF14^{F145S}$ compared with cells expressing only GFP (see also Table 1).

Table 1. Voltage-gated Na^+ currents in rat hippocampal neurons

Cells	Peak density (pA/pF)	$V_{1/2}$ (act) (mV)	k_{act} (mV)	$V_{1/2}$ (inact) (mV)	k_{inact} (mV)
GFP	−150 ± 15 (38)	−27 ± 1 (22) −33 ± 1	6.0 ± 0.3 (22) 3.6 ± 0.3	−60 ± 1 (27)	6.1 ± 0.2 (27)
FGF14	−242 ± 24 (17)* −61 ± 13	(13)** −22 ± 2	(13)***	−56 ± 1 (10)**	5.4 ± 0.2 (10) 8.0 ± 0.5
$FGF14^{F145S}$	(29)***	(9)**	6.4 ± 0.3 (9)	−66 ± 1 (9)**	(9)***

All values are means ± SEM; numbers in parentheses are the numbers of cells analyzed. Values are significantly different from those determined in cells expressing GFP alone at the *$p < 0.01$, **$p < 0.005$, and ***$p < 0.001$ levels.

were routinely recorded from all GFP-expressing ($n = 38$), $FGF14^{F145S}$-expressing ($n = 29$), and FGF14-expressing ($n = 17$) cells (Fig. 2). Peak Na_v current densities, however, were significantly ($p < 0.001$) lower in cells expressing $FGF14^{F145S}$ (−61 ± 13 pA/pF) than in cells expressing GFP (−150 ± 15 pA/pF) (Fig. 2*D*). Although peak Na_v current densities were reduced, expression of $FGF14^{F145S}$ did not measurably affect the kinetic properties of the currents. There were, however, small but statistically significant ($p < 0.005$) shifts in the voltage dependences of Na_v channel activation (approximately +5 mV depolarizing shift) and inactivation (−6 mV hyperpolarizing shift) in cells expressing $FGF14^{F145S}$ compared with cells expressing GFP (Fig. 2*E*, Table 1).

The effects of $FGF14^{F145S}$ expression on peak Na_v current densities were distinct from those produced by overexpression of wild-type FGF14 (Fig. 2*D*). Consistent with previous findings (Lou et al., 2005), Na_v current densities were, on average, increased by ~50% (Fig. 2*D*) in hippocampal neurons transfected with FGF14, to a mean ± SEM of 242 ± 24 pA/pF ($n = 17$), a value that is significantly ($p < 0.01$) higher than in cells expressing GFP (Table 1). Expression of wild-type FGF14 also resulted in small but statistically significant ($p < 0.005$) shifts in the voltage dependences of Na_v channel activation (approximately −6 mV hyperpolarizing shift) and inactivation (approximately +4 mV depolarizing shift) (Fig. 2*E*, Table 1). The effects of overexpression of wild-type FGF14 on peak Na_v current densities and on Na_v channel activation and inactivation therefore are opposite to those produced by expression of the FGF14 mutant protein $FGF14^{F145S}$ (Fig. 2*E*) (see Discussion).

Expression of $FGF14^{F145S}$ decreases the excitability of hippocampal neurons

To explore the functional consequences of the observed reductions in peak Na_v current densities in cells expressing $FGF14^{F145S}$, whole-cell current-clamp recordings were obtained from hippocampal neurons expressing $FGF14^{F145S}$, GFP, or wild-type FGF14. As demonstrated previously for wild-type (nontransfected) rat hippocampal neurons (Colbert and Pan, 2002; Clark et al., 2005; Meeks et al., 2005), action potentials, evoked in response to brief (2 ms) depolarizing current injections, in GFP-expressing cells rose rapidly to a maximal potential of approximately +50 mV, and repolarization was rapid (Fig. 3*A*). The waveforms of individual action potentials in cells expressing $FGF14^{F145S}$ were indistinguishable from those recorded in GFP-expressing cells, although more current was required to reach the threshold for action potential generation (Fig. 3*B*). In cells expressing FGF14 (Fig. 3*C*), action potential waveforms were also indistinguishable from those in GFP-expressing neurons (Fig. 3*A*). Further analyses revealed that mean ± SEM input resistances (Fig. 3*D*) and action potential durations (Fig. 3*E*) in GFP-, FGF14-, and $FGF14^{F145S}$-expressing neurons were not significantly different. The mean ± SEM current (444 ± 27 pA; $n = 13$) required to evoke single action potentials in $FGF14^{F145S}$-expressing cells (Fig. 3*F*), however, was significantly ($p < 0.001$) larger than in cells expressing GFP (331 ± 26 pA; $n = 25$) or FGF14 (354 ± 37 pA; $n = 8$).

In response to prolonged (500 ms) low-amplitude (10–100 pA) depolarizing current injections, GFP-expressing rat hippocampal neurons fired repetitively and at frequencies that varied with the stimulus strength (Fig. 4*A*,*B*). Repetitive firing was also readily evoked in FGF14-GFP-expressing neurons (Fig. 4*C*,*D*). The responses to prolonged current injections and the maximal firing frequencies were similar to those recorded in wild-type (GFP-expressing) neurons. In $FGF14^{F145S}$-expressing neurons, however, excitability was reduced (Fig. 4*E*,*F*). Similar to the responses to brief current injections (Fig. 3), larger currents

were required to evoke action potentials (and repetitive firing) in FGF14^{F145S}-expressing cells than in cells expressing GFP or wild-type FGF14 (Fig. 4*E*, Table 2). In addition, repetitive firing was markedly attenuated in FGF14^{F145S}-expressing cells, and ~70% of the cells fired fewer than four action potentials during 500 ms depolarizing current injections, regardless of the magnitude of injected current (Figs. 4*F*, 5*D*) ($p < 0$; 1, $n = 16$). Action potentials in FGF14^{F145S}-expressing cells were otherwise indistinguishable from those in GFP- and FGF14-expressing cells, displaying comparable voltage thresholds, amplitudes, and durations (Table 2).

If the only mode of action of FGF14^{F145S} was to reduce the number of available Na_v channels, then application of the specific Na_v channel blocker (Catterall et al., 2005) TTX at low (1–5) nanomolar concentrations should mimic the effects of FGF14^{F145S} on membrane excitability. Indeed, additional experiments revealed that exposure of GFP-expressing neurons to 1–5 nM TTX markedly increased the amplitudes of the currents required to evoke action potentials (Fig. 5*A–C*), consistent with blockade of a fraction of available Na_v channels. In addition, exposure to TTX decreased the number of action potentials recorded in response to prolonged (500 ms) depolarizing current injections (Fig. 5*D*), without significantly affecting the amplitudes or the durations of individual action potentials (Table 2). Thus, the deficits in neuronal excitability observed in FGF14^{F145S}-expressing neurons are mimicked by the application of low (1–5) nanomolar concentrations of TTX. At higher (≥10 nM) TTX concentrations, rat hippocampal neurons ceased firing altogether.

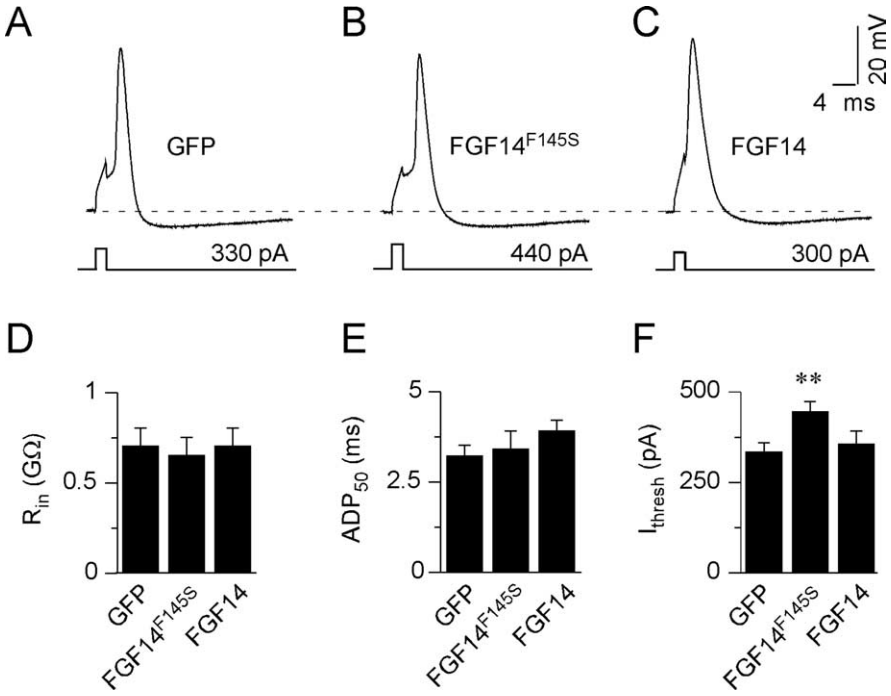

Figure 3. Expression of FGF14F145S reduces the excitability of hippocampal neurons. ***A–C***, Single action potentials, evoked by brief (2 ms) depolarizing current injections, were recorded from isolated (rat) hippocampal neurons expressing GFP (***A***), FGF14^{F145S}-GFP (***B***), or FGF14-GFP (***C***), as described in Materials and Methods. The amplitudes and durations of the injected currents are illustrated below the voltage records. Although larger-amplitude currents were required to evoke action potentials in FGF14^{F145S}-GFP-expressing cells (***B***) compared with FGF14-GFP-expressing (***C***) and GFP-expressing (***A***) cells, action potentials in all cells are brief and afterhyperpolarizations are pronounced. In addition, there are no significant differences in the waveforms of the action potentials in cells expressing FGF14^{F145S}-GFP (***B***) compared with cells expressing wild-type FGF14-GFP (***C***) or GFP (***A***). ***D***, ***E***, The input resistances (***D***) and the durations of single action potentials, measured at 50% repolarization (APD_{50}) (***E***), in FGF14^{F145S}-GFP-, FGF14-GFP-, and GFP-expressing cells are indistinguishable. ***F***, The mean ± SEM current (I_{thresh}) required to elicit single action potentials, however, was significantly (**$p < 0.005$) higher in cells expressing FGF14^{F145S}-GFP ($n = 13$) compared with cells expressing GFP ($n = 25$) or wild-type FGF14-GFP ($n = 8$).

FGF14^{F145S} functions as a dominant negative

Previous studies have demonstrated that wild-type FGF14 coimmunoprecipitates with $Na_v1.1$ and $Na_v1.5$ α subunits (Lou et al., 2005). To determine whether FGF14 (and/or FGF14^{F145S}) also interacts with the major Na_v α subunit in hippocampal neurons, $Na_v1.2$ (Schaller and Caldwell, 2000), myc-tagged *Fgf14* (*Fgf14-myc*), or *Fgf14^{F145S}* (*Fgf14^{F145S}-myc*) was transiently transfected into HEK-293 cells stably expressing $Na_v1.2$ (HEK-$Na_v1.2$ cells). In addition, control experiments were performed on cells transiently transfected with *hSpry-myc*, which encodes an unrelated protein that has also been myc tagged at the C terminus. Using anti-myc agarose beads, FGF14-myc (as well as FGF14^{F145S}-myc and hSpry-myc) was efficiently immunoprecipitated from extracts of transiently transfected HEK-$Na_v1.2$ cells (Fig. 6*A*). In addition, similar to the previously demonstrated interactions between FGF14 and the $Na_v1.1$ and $Na_v1.5$ α subunits (Lou et al., 2005), $Na_v1.2$ coimmunoprecipitated with FGF14-myc in a dose-dependent manner (Fig. 6*A*,*B*). In contrast, $Na_v1.2$ did not coimmunoprecipitate with FGF14^{F145S}-myc (Fig. 6*C*), suggesting that the observed effects of FGF14^{F145S} on hippocampal Na_v currents (Fig. 2) likely do not result from a direct interaction between FGF14^{F145S} and Na_v α subunits. Control experiments revealed that $Na_v1.2$ also does not coimmunoprecipitate from cells expressing the unrelated protein hSpry-myc (Fig. 6*A*,*C*). Together, these results suggest that the effects of FGF14^{F145S} on hippocampal Na_v channels likely are indirect.

To test the hypothesis that FGF14^{F145S} acts by interfering with the interaction between wild-type FGF14 and Na_v channel α subunits, HEK-$Na_v1.2$ cells were transiently transfected with *Fgf14^{F145S}-Gfp* and *Fgf14-myc*, and immunoprecipitations were again performed with anti-myc agarose beads. Control experiments were, as described above, also performed on cells transiently transfected with the *hSpry-myc* construct. As illustrated in Figure 7*A*, substantially less $Na_v1.2$ coimmunoprecipitated from cells cotransfected with *Fgf14^{F145S}-Gfp* and *Fgf14-myc* compared with cells transfected with the *Fgf14-myc* construct alone. Quantification of immunoprecipitated $Na_v1.2$ protein in blots from six independent experiments demonstrated that the fraction of $Na_v1.2$ coimmunoprecipitating with FGF14-myc was progressively reduced as the amount of transfected *Fgf14^{F145S}-Gfp* was increased (Fig. 7*B*). Importantly, the expression levels of FGF14-myc in cells with and without FGF14^{F145S}-GFP were similar (Fig. 7*A*), suggesting that neither the expression nor the stability of the wild-type FGF14 protein was affected by the presence of the FGF14^{F145S} mutant protein.

The reduction in immunoprecipitated $Na_v1.2$ protein (with the anti-myc antibody) from HEK-$Na_v1.2$ cells cotransfected with *Fgf14-myc* and *Fgf14^{F145S}-Gfp* (Fig. 7*A*,*B*) suggested that

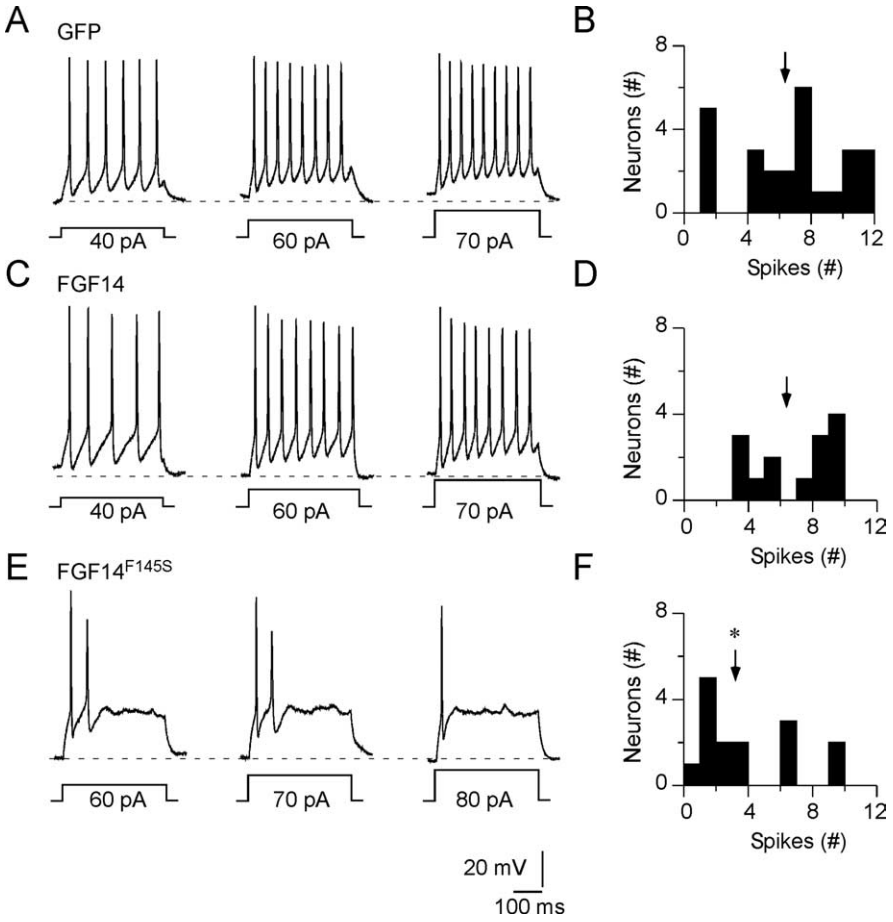

Figure 4. Expression of FGF14^{F145S} attenuates repetitive firing in hippocampal neurons. Repetitive firing in isolated hippocampal neurons expressing GFP (***A***), FGF14-GFP (***C***), or FGF14^{F145S}-GFP (***E***) was evoked in response to prolonged (500 ms) depolarizing current injections, as described in Materialss and Methods. Representative examples are illustrated, and the amplitudes of the injected currents are illustrated below the voltage records. ***A***, Hippocampal neurons expressing GFP typically fire repetitively and at rates that vary with the amplitude of the injected current. ***B***, Distribution of maximal number of action potentials evoked in individual GFP-expressing cells ($n = 27$) during 500 ms, 90 pA current injections. ***C***, The repetitive firing properties of cells expressing FGF14-GFP are similar (to those of cells expressing GFP), with average firing rates increasing with the stimulus intensity. ***D***, The distribution of the maximal number of evoked action potentials in FGF14-GFP-expressing cells ($n = 13$) is similar to cells expressing GFP (***B***). ***E***, Repetitive firing is attenuated markedly in neurons expressing FGF14^{F145S} ($n = 16$), and repetitive firing rates in most FGF14^{F145S}-expressing cells do not increase substantially in response to increasing the amplitudes of the injected currents. ***F***, Histogram showing the distribution of the maximal numbers of action potentials fired (during 500 ms depolarizing 90 pA current injections) in FGF14^{F145S}-GFP-expressing cells is skewed to the left (fewer action potentials) compared with cells expressing GFP (***B***) or FGF14-GFP (***D***). The mean number of action potentials evoked in FGF14^{F145S}-GFP-expressing cells is significantly (*$p < 0.01$) lower than in GFP or FGF14-GFP expressing cells. Arrows in ***B***, ***D***, and ***F*** indicate the mean number of action potentials elicited in response to 500 ms, 90 pA current injections.

Table 2. Passive and active membrane properties of rat hippocampal neurons

	C_m (pF)	R_{in} (GΩ)	V_m (mV)	$I_{threshold}$ (pA)	$V_{threshold}$ (mV)	APA (mV)	APD_{50} (ms)
GFP ($n = 30$)	44 ± 3	0.7 ± 0.1	−56 ± 1	38 ± 6	−28 ± 0.9	81 ± 2	3.7 ± 0.3
FGF14 ($n = 13$)	53 ± 4	0.7 ± 0.1	−55 ± 1	34 ± 6	−28 ± 1.4	78 ± 3	4.4 ± 0.2
FGF14^{F145S} ($n = 16$)	49 ± 5	0.7 ± 0.1	−58 ± 1	62 ± 7***	−26 ± 1.3	76 ± 4	4.4 ± 0.4
GFP ($n = 6$)	52 ± 6	0.7 ± 0.1	−57 ± 2	24 ± 4	−30 ± 0.5	89 ± 8	3.8 ± 1.2
+1 nM TTX ($n = 4$)				56 ± 8*	−30 ± 0.9	87 ± 5	3.1 ± 0.3
+5 nM TTX ($n = 4$)				88 ± 6**	−25 ± 3.7	87 ± 1	4.1 ± 0.5

All values are means ± SEM. APA, Action potential amplitude; APD_{50}, action potential duration at 50% repolarization. ***$p < 0.001$, significantly different from the values measured in GFP- or FGF14-expressing cells; **$p < 0.005$ and *$p < 0.01$, significantly different from those measured in control recordings in the absence of TTX.

FGF14^{F145S} might interfere with the interaction between wild-type FGF14 and $Na_v1.2$ by associating with FGF14. To test this hypothesis directly, *Fgf14-myc* and *Fgf14^{F145S}-Gfp* were cotransfected into HEK-293 cells, and whole-cell lysates were immunoprecipitated using the anti-myc agarose beads. Control experiments were performed on *Fgf14-GFP* or *Fgf14^{F145S}-GFP* cells cotransfected with a construct encoding a myc-tagged glutamate receptor subunit, *myc-GluR6*. As illustrated in Figure 7*C*, FGF14^{F145S}-GFP, like FGF14-GFP, coimmunoprecipitated with FGF14-myc, suggesting that the single amino acid mutation, F145S, which is present in the conserved FGF core domain, did not affect the ability of the FGF14 protein to self-associate. FGF14^{F145S}-GFP also coimmunoprecipitated with FGF14-myc when coexpressed in HEK-$Na_v1.2$ cells (Fig. 7*D*), findings consistent with the suggestion that the mutant FGF14^{F145S} protein interacts with wild-type FGF14, disrupting the interaction (of wild-type FGF14) with $Na_v1.2$ (Fig. 7*A*,*B*) and, consequently, the subcellular distribution of $Na_v1.2$ channels (see Discussion).

This model of FGF14^{F145S} action, together with the finding that heterologously expressed FGF14-GFP is enriched at the AIS (Fig. 1), suggests that endogenous FGF14, and potentially other iFGFs, are also enriched at the AIS. In collaboration with the National Institute of Neurological Disorders and Stroke–National Institute of Mental Health-sponsored NeuroMabs Facility at the University of California at Davis, we have recently developed a mouse monoclonal antibody targeted against FGF14 (see Materials and Methods). This reagent has now allowed visualization of endogenous FGF14 in primary hippocampal neurons (Fig. 8). As illustrated in Figure 8*A–C*, robust expression of FGF14 is evident in MAP2-negative processes (axons). In addition, FGF14 expression is colocalized with βIV-spectrin (Fig. 8*D–F*), a structural protein that is highly enriched in the AIS and that regulates sodium channel clustering (at the AIS) through ankyrin-G (Komada and Soriano, 2002; Nishimura et al., 2007).

Discussion

The results presented here demonstrate that expression of the human FGF14 mutant protein FGF14^{F145S} reduces the expression of Na_v α subunits at the AIS, attenuates Na_v current densities, and decreases the excitability of hippocampal neurons. Although the apparent regulation of Na_v current densities and Na_v channel subcellular localization might reflect independent functions of FGF14, the phenotypic consequences of expression of FGF14^{F145S} on neuronal firing properties are clearly consistent with the observed de-

creases in functional Na_v channel densities observed in the voltage-clamp experiments. A reduction in the number of functional Na_v channels, for example, would account for the findings that larger currents ($I_{threshold}$) were required to evoke action potentials and that maximal firing frequencies were reduced in cells expressing $FGF14^{F145S}$. In addition, the changes in excitability identified in hippocampal neurons expressing $FGF14^{F145S}$ were mimicked by applications of low concentrations (1–5 nM) of the specific Na_v channel blocker TTX (Catterall et al., 2005). The currents required to evoke action potentials were increased, and repetitive firing was attenuated in hippocampal neurons after exposure to 1–5 nM TTX. As would be expected, action potentials could not be generated in cells exposed to higher concentrations (≥10 nM) of TTX.

Importantly, the passive membrane properties of hippocampal neurons expressing $FGF14^{F145S}$ and the waveforms of evoked action potentials in these cells (Table 2) were indistinguishable from those measured in wild-type neurons. These observations suggest that other voltage-dependent currents, such as Ca^{2+} and K^+ currents, which are also expressed in hippocampal neurons and contribute to the regulation of membrane excitability (Reyes, 2001), are not affected by the expression of $FGF14^{F145S}$. Consistent with this hypothesis, voltage-clamp recordings from GFP-, FGF14-GFP-, and $FGF14^{F145S}$-GFP-expressing cells revealed no significant differences in the densities or the properties of repolarizing voltage-gated or inwardly rectifying K^+ channels (data not shown). Thus, the changes in membrane excitability described here in hippocampal neurons expressing $FGF14^{F145S}$ are consistent with a specific effect of the mutant protein on the expression/functioning of Na_v channels. Interestingly, a recent study of granule cells in cerebellar slices from mice lacking FGF12 (*Fgf12−/−*) and/or FGF14 (*Fgf14−/−*) revealed marked changes in granule cell excitability that were also attributed to altered Na_v channel functioning (Goldfarb et al., 2007).

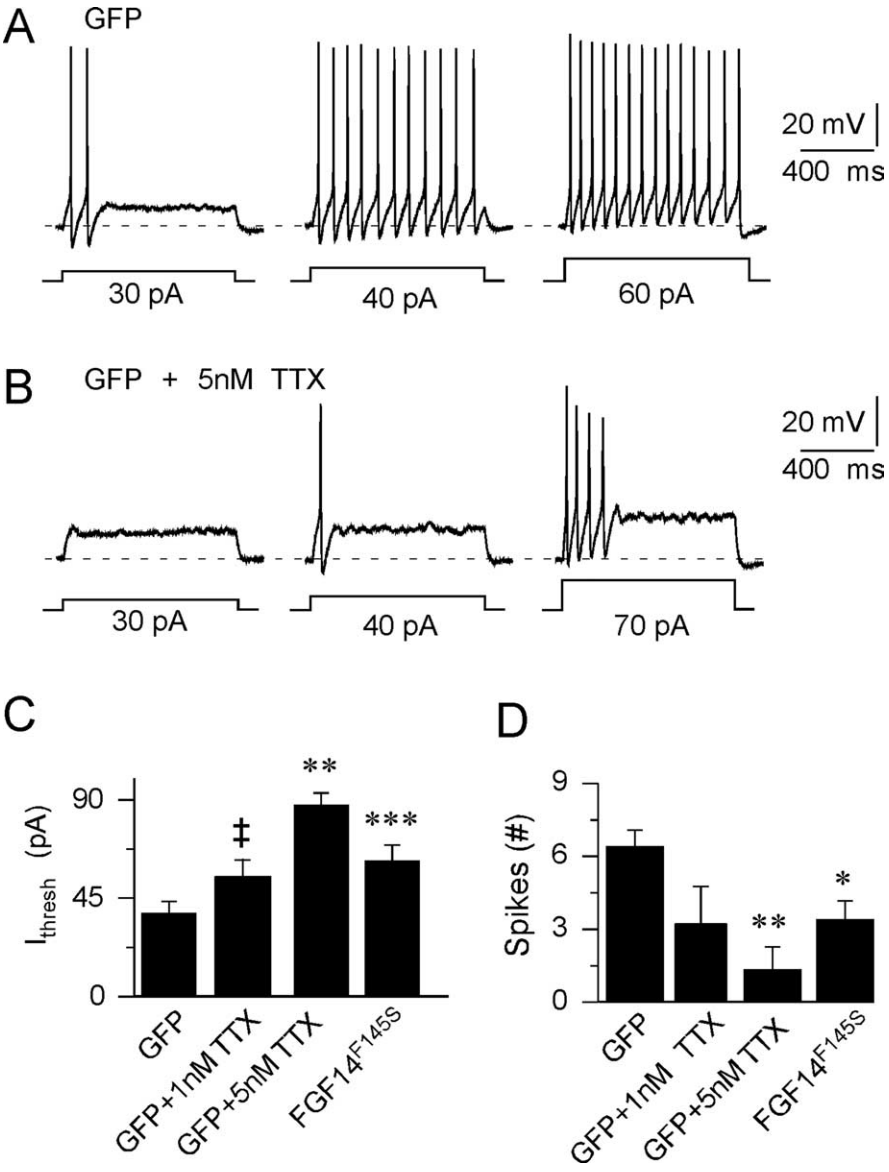

Figure 5. Application of low concentrations of TTX reduces excitability and attenuates repetitive firing in hippocampal neurons, mimicking the effects of $FGF14^{F145S}$ expression. Action potentials were recorded, as described in the legend to Figure 4, from GFP-expressing (wild-type) hippocampal neurons before and after local applications of 1–5 nM TTX. ***A***, Representative action potentials recorded from a GFP-expressing hippocampal pyramidal neuron in response to increasing depolarizing current injections. ***B***, After application of 5 nM TTX, more current was required to evoke action potentials to fire, and repetitive firing was reduced. ***C***, ***D***, The effects of TTX on firing properties are similar to those seen in cells expressing $FGF14^{F145S}$-GFP. The mean ± SEM ($n = 4$) current (***C***) required to evoke action potentials was increased significantly (**$p < 0.01$; ***$p < 0.001$), whereas the mean ± SEM number of spikes (***D***) evoked (during 1 s depolarizing current injections) was reduced significantly (*$p < 0.01$); **$p < 0.01$ in GFP-expressing cells exposed to 5 nM TTX. Exposure to 1 nM TTX ($n = 4$) also increased the mean ± SEM current required to evoke action potentials ($^{\ddagger}p = 0.05$) in GFP-expressing cells. Repetitive firing was also reduced after exposure to 1 nM TTX, although the mean ± SEM number of spikes evoked was not statistically lower than control. The mean ± SEM current required to evoke action potentials (***C***) and the mean ± SEM maximal number of spikes evoked during 1 s depolarizing current injections in $FGF14^{F145S}$-expressing cells (***D***) are plotted here for comparison.

$FGF14^{F145S}$ acts as a dominant negative, interfering with the functioning of FGF14

The electrophysiological effects of $FGF14^{F145S}$ expression in hippocampal neurons are distinct from those produced by overexpression of wild-type FGF14, which augments Na_v current densities, but does not measurably affect the firing properties of hippocampal neurons. The lack of effect of FGF14 overexpression on the firing properties of hippocampal neurons (Fig. 4) despite observed increases in Na_v current densities (Fig. 2) suggests that the number of functional Na_v channels expressed in hippocampal neurons is already in excess of the number required to maintain maximal firing. The biochemical studies presented here also demonstrate that, unlike wild-type FGF14, heterologously expressed $FGF14^{F145S}$ does not coimmunoprecipitate with, and therefore does not interact directly with, neuronal $Na_v1.2$ α subunits. The mutant $FGF14^{F145S}$ protein, like wild-type FGF14 protein, however, coimmunoprecipitated with wild-type FGF14 and, in addition, affected the association of wild-type FGF14 with $Na_v1.2$ α subunits. Together, these observations sug-

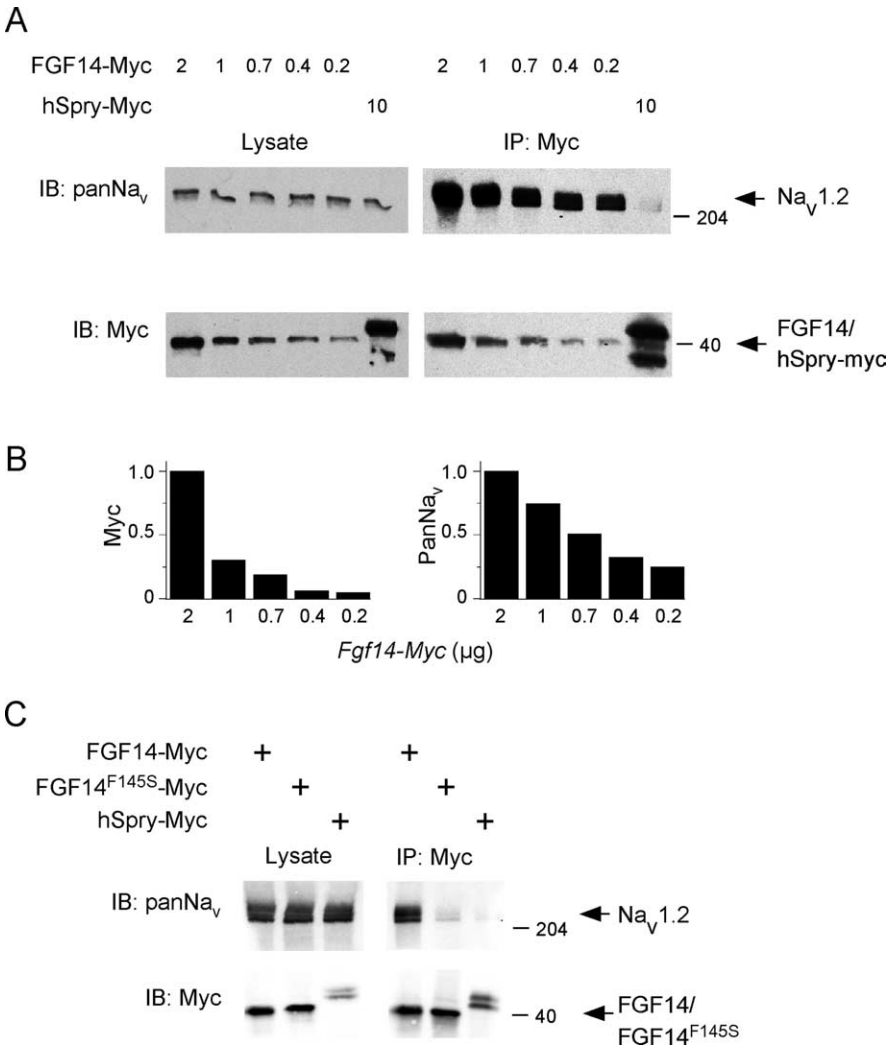

Figure 6. FGF14^{F145S} does not interact directly with Na$_v$ α subunits. ***A***, HEK-Na$_v$1.2 cells were transiently transfected with varying concentrations (2–0.2 μg) of *Fgf14-myc* or with the (negative) control plasmid *hSpry-myc* (10 μg). Western blots of whole-cell lysates (left panels) revealed a constant level of Na$_v$1.2 expression and variable levels of expression of FGF14-myc, paralleling the concentrations of *Fgf14-myc* used in the transfection (left). After immunoprecipitation of cell extracts with anti-myc agarose beads (IP: Myc), immunoblots (IB) were probed with either an anti-myc or an anti-Pan Na$_v$ α subunit antibody (right). As is evident, Na$_v$1.2 coimmunoprecipitates with the anti-myc agarose beads from cells expressing FGF14-myc but not from cells expressing hSpry-myc. ***B***, In addition, quantification of the relative intensities of the anti-myc and anti-Na$_v$1.2 bands from the Western blots of the coimmunoprecipitated (Na$_v$1.2 and FGF14) proteins revealed parallel efficiencies as a function of the amount of *Fgf14-myc* used in the transfections. ***C***, HEK-Na$_v$1.2 cells were transiently transfected with *Fgf14-myc*, *Fgf14^{F145S}-myc*, or with the *hSpry-myc* control plasmid. Western blots of lysates from these cells (left) revealed uniform levels of Na$_v$1.2 and robust expression of FGF14-myc, FGF14^{F145S}-myc, or hSpry-myc. After immunoprecipitations with anti-myc beads (IP: Myc), immunoblots (IB) were performed (right) using the anti-myc or anti-Pan Na$_v$ α subunit antibodies. In contrast to FGF14-myc (***A***), Na$_v$1.2 was not coimmunoprecipitated from cells expressing FGF14^{F145S}-myc (or hSpry-myc) using anti-myc agarose beads.

gest that endogenous FGF14 likely functions as an oligomeric protein and, furthermore, that FGF14^{F145S}, by interacting with wild-type FGF14 protein, acts as a dominant negative to disrupt the association between (wild-type) FGF14 and Na$_v$ channel α subunits.

The results presented here also suggest that the single missense mutation, F145S, in the *FGF14* gene in individuals afflicted with the autosomal-dominant neurodegenerative disorder SCA27 results in a loss of function by blocking the interaction(s) between wild-type FGF14 and Na$_v$ α subunits, thereby reducing the number of functional Na$_v$ channels and reducing neuronal excitability. Based on these observations, expression of FGF14^{F145S} would be expected to result in phenotypes in brain areas where FGF14 is highly expressed, such as the cerebellum, hippocampus, and striatum (Wang et al., 2000). Alterations in Na$_v$ channel expression/function in these brain regions might contribute to the progressive ataxia, cognitive impairments, and motor deficits seen in SCA27 individuals (Van Swieten et al., 2003). Previous studies have demonstrated that *Fgf14*$^{-/-}$ mice display multiple neurological phenotypes, including ataxia and cognitive impairment (Wang et al., 2002; Wozniak et al., 2007; Xiao et al., 2007), that are remarkably similar to those observed in SCA27 patients, further supporting the proposed loss-of-function model for FGF14^{F145S}.

Intracellular FGFs as novel regulators of neuronal membrane excitability

When heterologously expressed in hippocampal neurons, FGF14-GFP was found highly enriched at the AIS, colocalized with endogenous Na$_v$ channels. Consistent with this expression pattern, endogenous FGF14, detected with a newly developed (anti-FGF14) specific monoclonal antibody, is readily detected in isolated hippocampal neurons in MAP2-negative processes and colocalized with βIV-spectrin at the AIS. This pattern of endogenous FGF14 expression, together with the observations that the FGF14^{F145S} mutant protein does not interact with Na$_v$ channels or localize at the AIS, strongly suggests that FGF14^{F145S} acts by disrupting the interaction between FGF14 and Na$_v$ channel α subunits at the AIS. Additional experiments are needed to test this hypothesis directly.

The experiments here also revealed that, in neurons expressing FGF14^{F145S}, Na$_v$ α subunit expression at the AIS was reduced. Because the biochemical data presented demonstrate that FGF14^{F145S} interacts with wild-type FGF14 (and not Na$_v$ α subunits), these results suggest that FGF14^{F145S} interferes with endogenous FGF14 interactions with Na$_v$ α subunits at the AIS in hippocampal neurons and, through this mechanism, attenuates neuronal excitability by interfering with the trafficking or the stabilization of Na$_v$ channels. Previous studies have demonstrated that other iFGFs, notably FGF12 and FGF13, also interact with Na$_v$ α subunits in heterologous expression systems, differentially affecting cell-surface Na$_v$ current densities and the voltage dependences of Na$_v$ channel activation and inactivation (Liu et al., 2001, 2003; Wittmack et al., 2004; Rush et al., 2006). The other iFGFs therefore may also play similar functional roles in the regulation of Na$_v$ channel functioning, either alone or in combination with FGF14. Studies focused on exploring potential redundancy between various members of the iFGF family will be necessary to test this hypothesis directly.

Wild-type FGF14 could regulate neuronal Na$_v$ channel ex-

pression, localization, and functioning by a variety of different mechanisms. Interestingly, the functional effects of FGF14 are reminiscent of the modulatory effects of Na_v channel accessory (β) subunits, which have been shown to affect Na_v channel assembly, surface expression, and (biophysical) properties (Isom et al., 1994; Catterall, 2000; Isom, 2002), and are similar to those of FGF14 (and the other iFGFs). These observations suggest the interesting possibility that the iFGFs might modulate Na_v α–Na_v β subunit–subunit interactions. It is certainly also possible that the iFGFs exert direct (or indirect) effects on the biosynthesis and/or the stability or the trafficking of assembled Na_v channels (Garrido et al., 2001). Indeed, FGF12, FGF13 (Schoorlemmer and Goldfarb, 2002), and FGF14 (J.-Y. Lou and D. M. Ornitz, unpublished data) interact with JIP-2, a component of the kinesin-dependent cargo system involved in axonal transport (Verhey et al., 2001; Hirokawa and Takemura, 2005). Thus, FGF14 (and other iFGFs) might play a role in directing Na_v channel localization to the AIS through a kinesin-mediated pathway. Targeting motifs required for axonal and AIS localization are found in the C-terminal tails and in the II–III intracellular loops of Na_v α subunits (Garrido et al., 2001, 2003a,b). Because FGF12 (Liu et al., 2001, 2003), FGF13 (Wittmack et al., 2004) and FGF14 (Lou et al., 2005) interact with the C termini of some Na_v α subunits, FGF14 (and the other iFGFs) might affect the function of domains important for Na_v α subunit subcellular localization. For example, FGF14 might affect the interaction of other proteins, such as ankyrin-G, which is required for proper Na_v α subunit localization (Garrido et al., 2003a). Clearly, studies focused on exploring the possibility that FGF14 interacts directly with ankyrin-G and/or affects the interactions between ankyrin-G and Na_v channel α subunits, as well as studies focused on exploring the molecular mechanisms involved in mediating the decrease expression of Na_v channels at the AIS observed on expression of $FGF14^{F145S}$, are needed to test each of these hypotheses directly.

In addition to providing molecular insights into the mechanisms involved in mediating the action of the SCA27 mutant $FGF14^{F145S}$ protein, the results presented here clearly suggest that expression of $FGF14^{F145S}$ would be expected to have dramatic physiological consequences. A decrease in the number of Na_v channels at the AIS, for example, is expected to inhibit action potential initiation (Meeks et al., 2005) and affect both the forwardpropagation and the backpropagation of action potentials. Decreased efficacy of forward action potential propagation, in turn, would be expected to reduce the reliability of synaptic transmission (Debanne, 2004) and synaptic remodeling (Clark and Hausser, 2006), whereas decreased fidelity of backpropagat-

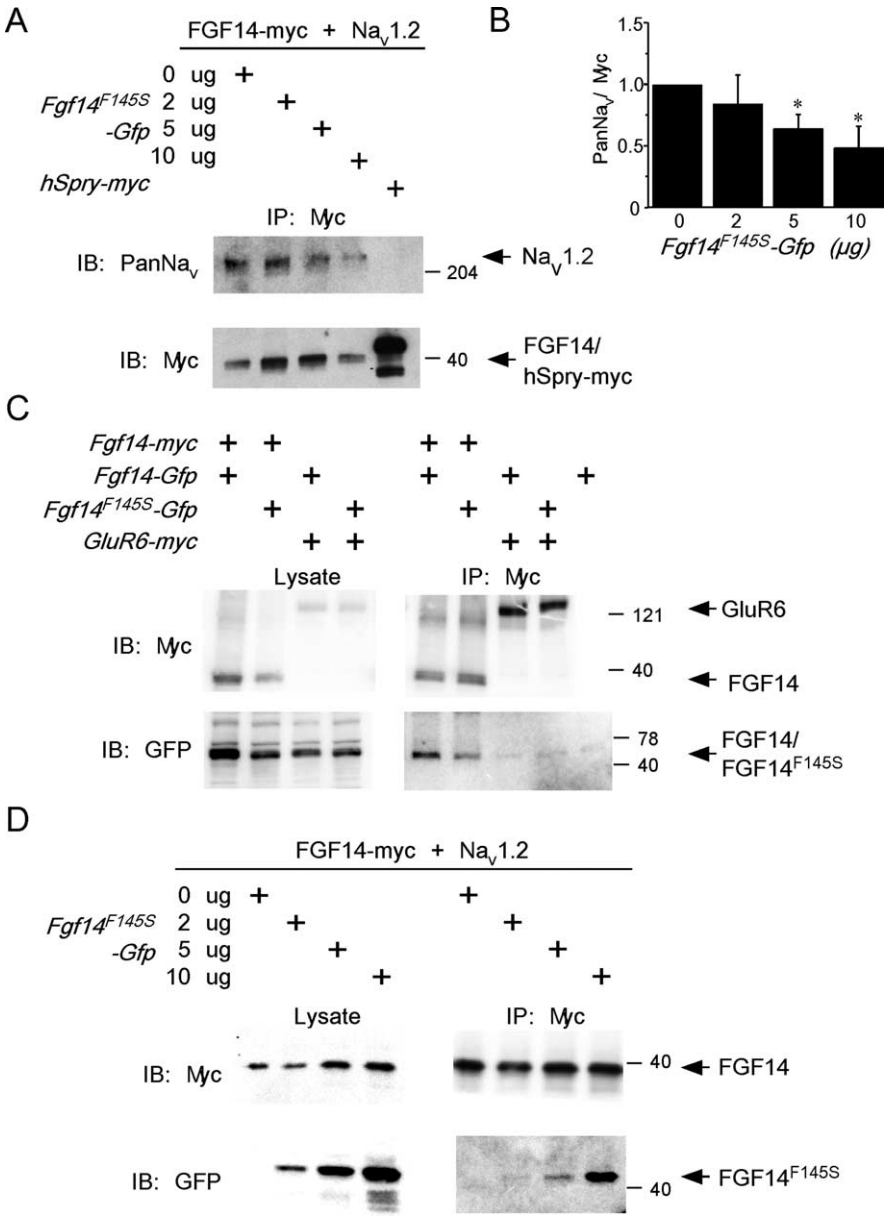

Figure 7. $FGF14^{F145S}$ disrupts the interaction between FGF14 and $Na_v1.2$ and coimmunoprecipitates with wild-type FGF14. ***A***, HEK-$Na_v1.2$ cells were transiently transfected with *Fgf14-myc* and increasing amounts of *Fgf14^{F145S}-Gfp* or with the (negative) control *hSpry-myc* construct. After immunoprecipitation with anti-myc agarose beads (IP: Myc), immunoblots (IB) were performed with either the anti-Pan Na_v α subunit or the anti-myc monoclonal antibody (left). As is evident, increasing the amount of $FGF14^{F145S}$–GFP reduced the amount of $Na_v1.2$ that coimmunoprecipitated with the anti-myc beads (FGF14). As was also illustrated in Figure 6, $Na_v1.2$ does not coimmunoprecipitate with hSpry-myc. ***B***, Densitometric ratio of coimmunoprecipitated $Na_v1.2$/FGF14-myc plotted as a function of the *Fgf14^{F145S}-Gfp* used in the transfections. These analyses revealed that increasing the amount of *Fgf14^{F145S}-Gfp* significantly ($*p < 0.01$) reduced the amount of $Na_v1.2$ coprecipitating with anti-myc agarose beads. ***C***, HEK-293 cells were transiently transfected with *Fgf14-myc* (or with the control plasmid *myc-GluR6*) and either *Fgf14-Gfp* or *Fgf14^{F145S}-Gfp*. Western blots of whole-cell lysates (left) confirmed expression of the tagged constructs. Whole-cell lysates were immunoprecipitated with anti-myc agarose beads (IP: Myc), and immunoblots (IB) were performed using either the anti-myc or anti-GFP antibody (right). Both FGF14-GFP and $FGF14^{F145S}$-GFP were coimmunoprecipitated with the myc-tagged FGF14. The association appears to be specific for FGF14 because myc-GluR6 did not coimmunoprecipitate with either FGF14-GFP or $FGF14^{F145S}$-GFP. ***D***, The interaction between $FGF14^{F145S}$-GFP and FGF14-myc was also evident in the presence of $Na_v1.2$. HEK-$Na_v1.2$ cells were transiently transfected with *Fgf14-myc* and with increasing concentrations of *Fgf14^{F145S}-Gfp*. Western blots of lysates from these cells (left) revealed expression of FGF14-myc and increasing concentrations of $FGF14^{F145S}$-GFP. In addition, $FGF14^{F145S}$-GFP was coimmunoprecipitated with FGF14-myc from these cells (IP: Myc) using anti-myc agarose beads (right).

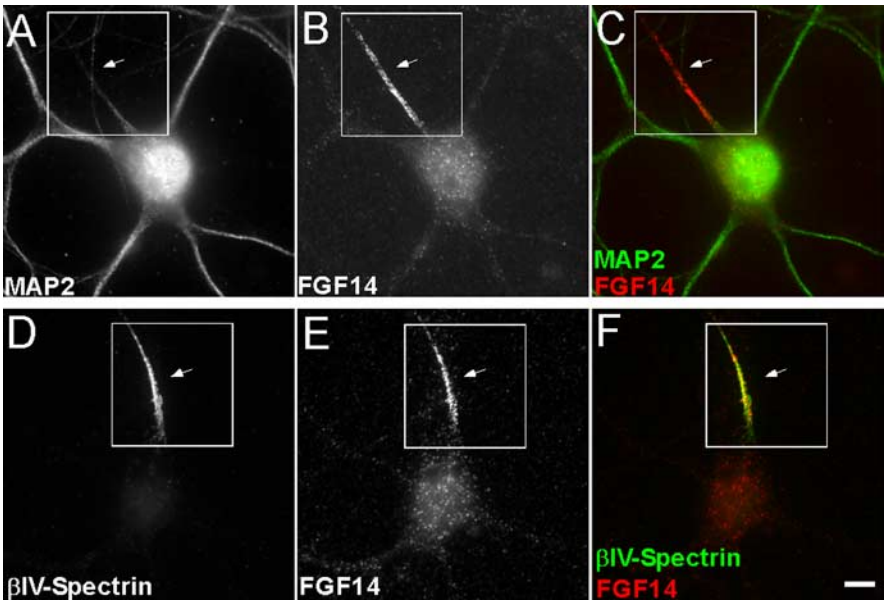

Figure 8. Endogenous FGF14 is readily detected in isolated rat hippocampal neurons, concentrated in the AIS. Fluorescence images of rat hippocampal neurons at 14 DIV show double labeling for FGF14 and either MAP2 (***A–C***) or βIV-spectrin (***D–F***). FGF14 is shown in red, whereas MAP2 and βIV-spectrin are shown in green in the overlay images in ***C*** and ***F***. As is evident, FGF14 staining was present in MAP2-negative processes (***C***), colocalized with βIV-spectrin (***F***) at the AIS (arrows). Scale bar, 10 μm.

ing action potentials would be expected to affect dendritic signal integration (Waters et al., 2005; Sjostrom and Hausser, 2006). Interestingly, loss of FGF14 in *Fgf14*$^{-/-}$ mice resulted in decreased frequency of mEPSCs and attenuation of long-term potentiation at CA3–CA1 synapses in the hippocampus (Xiao et al., 2007). Additional studies focused on exploring directly the effects of FGF14^{F145S} on synaptic functioning and synaptic plasticity will be of interest.

References

Bechtold DA, Smith KJ (2005) Sodium-mediated axonal degeneration in inflammatory demyelinating disease. J Neurol Sci 233:27–35.

Catterall WA (2000) From ionic currents to molecular mechanisms: the structure and function of voltage-gated sodium channels. Neuron 26:13–25.

Catterall WA, Goldin AL, Waxman SG (2005) International Union of Pharmacology. XLVII. Nomenclature and structure-function relationships of voltage-gated sodium channels. Pharmacol Rev 57:397–409.

Clark B, Hausser M (2006) Neural coding: hybrid analog and digital signalling in axons. Curr Biol 16:R585–R588.

Clark BA, Monsivais P, Branco T, London M, Hausser M (2005) The site of action potential initiation in cerebellar Purkinje neurons. Nat Neurosci 8:137–139.

Colbert CM, Pan E (2002) Ion channel properties underlying axonal action potential initiation in pyramidal neurons. Nat Neurosci 5:533–538.

Coussen F, Normand E, Marchal C, Costet P, Choquet D, Lambert M, Mege RM, Mulle C (2002) Recruitment of the kainate receptor subunit glutamate receptor 6 by cadherin/catenin complexes. J Neurosci 22:6426–6436.

Debanne D (2004) Information processing in the axon. Nat Rev Neurosci 5:304–316.

Fache MP, Moussif A, Fernandes F, Giraud P, Garrido JJ, Dargent B (2004) Endocytotic elimination and domain-selective tethering constitute a potential mechanism of protein segregation at the axonal initial segment. J Cell Biol 166:571–578.

Garrido JJ, Fernandes F, Giraud P, Mouret I, Pasqualini E, Fache MP, Jullien F, Dargent B (2001) Identification of an axonal determinant in the C-terminus of the sodium channel Na(v)1.2. EMBO J 20:5950–5961.

Garrido JJ, Giraud P, Carlier E, Fernandes F, Moussif A, Fache MP, Debanne D, Dargent B (2003a) A targeting motif involved in sodium channel clustering at the axonal initial segment. Science 300:2091–2094.

Garrido JJ, Fernandes F, Moussif A, Fache MP, Giraud P, Dargent B (2003b) Dynamic compartmentalization of the voltage-gated sodium channels in axons. Biol Cell 95:437–445.

Goldfarb M (2005) Fibroblast growth factor homologous factors: evolution, structure, and function. Cytokine Growth Factor Rev 16:215–220.

Goldfarb M, Schoorlemmer J, Williams A, Diwakar S, Wang Q, Huang X, Giza J, Tchetchik D, Kelley K, Vega A, Matthews G, Rossi P, Ornitz DM, D'Angelo E (2007) Fibroblast growth factor homologous factors control neuronal excitability through modulation of voltage-gated sodium channels. Neuron 55:449–463.

Goslin K, Asmussen H, Banker G (1998) Rat hippocampal neurons in low-density culture. In: Culturing nerve cells (Banker G, Goslin K, eds), pp 339–370. Cambridge, MA: MIT.

Hirokawa N, Takemura R (2005) Molecular motors and mechanisms of directional transport in neurons. Nat Rev Neurosci 6:201–214.

Isom LL (2002) Beta subunits: players in neuronal hyperexcitability? Novartis Found Symp 241:124-138; discussion 138–143, 226–232.

Isom LL, De Jongh KS, Catterall WA (1994) Auxiliary subunits of voltage-gated ion channels. Neuron 12:1183–1194.

Itoh N, Ornitz DM (2004) Evolution of the *Fgf* and *Fgfr* gene families. Trends Genet 20:563–569.

Khaliq ZM, Raman IM (2006) Relative contributions of axonal and somatic Na channels to action potential initiation in cerebellar Purkinje neurons. J Neurosci 26:1935–1944.

Komada M, Soriano P (2002) [Beta]IV-spectrin regulates sodium channel clustering through ankyrin-G at axon initial segments and nodes of Ranvier. J Cell Biol 156:337–348.

Liu C, Dib-Hajj SD, Waxman SG (2001) Fibroblast growth factor homologous factor 1B binds to the C terminus of the tetrodotoxin-resistant sodium channel rNav1.9a (NaN). J Biol Chem 276:18925–18933.

Liu CJ, Dib-Hajj SD, Renganathan M, Cummins TR, Waxman SG (2003) Modulation of the cardiac sodium channel Na(v)1.5 by fibroblast growth factor homologous factor 1B. J Biol Chem 278:1029–1036.

Lou JY, Laezza F, Gerber BR, Xiao M, Yamada KA, Hartmann H, Craig AM, Nerbonne JM, Ornitz DM (2005) Fibroblast growth factor 14 is an intracellular modulator of voltage-gated sodium channels. J Physiol (Lond) 569:179–193.

Manto MU (2005) The wide spectrum of spinocerebellar ataxias (SCAs). Cerebellum 4:2–6.

Meeks JP, Jiang X, Mennerick S (2005) Action potential fidelity during normal and epileptiform activity in paired soma-axon recordings from rat hippocampus. J Physiol (Lond) 566:425–441.

Meisler MH, Kearney JA (2005) Sodium channel mutations in epilepsy and other neurological disorders. J Clin Invest 115:2010–2017.

Nishimura K, Akiyama H, Komada M, Kamiguchi H (2007) betaIV-spectrin forms a diffusion barrier against L1CAM at the axon initial segment. Mol Cell Neurosci 34:422–430.

Olsen SK, Garbi M, Zampieri N, Eliseenkova AV, Ornitz DM, Goldfarb M, Mohammadi M (2003) Fibroblast growth factor (FGF) homologous factors share structural but not functional homology with FGFs. J Biol Chem 278:34226–34236.

Ornitz DM, Itoh N (2001) Fibroblast growth factors. Genome Biol 2:REVIEWS3005.

Reyes A (2001) Influence of dendritic conductances on the input-output properties of neurons. Annu Rev Neurosci 24:653–675.

Rush AM, Wittmack EK, Tyrrell L, Black JA, Dib-Hajj SD, Waxman SG (2006) Differential modulation of sodium channel Na(v)1.6 by two members of the fibroblast growth factor homologous factor 2 subfamily. Eur J Neurosci 23:2551–2562.

Schaller KL, Caldwell JH (2000) Developmental and regional expression of

sodium channel isoform NaCh6 in the rat central nervous system. J Comp Neurol 420:84–97.

Schoorlemmer J, Goldfarb M (2002) Fibroblast growth factor homologous factors and the islet brain-2 scaffold protein regulate activation of a stress-activated protein kinase. J Biol Chem 277:49111–49119.

Sjostrom PJ, Hausser M (2006) A cooperative switch determines the sign of synaptic plasticity in distal dendrites of neocortical pyramidal neurons. Neuron 51:227–238.

Smallwood PM, Munoz-Sanjuan I, Tong P, Macke JP, Hendry SH, Gilbert DJ, Copeland NG, Jenkins NA, Nathans J (1996) Fibroblast growth factor (FGF) homologous factors: new members of the FGF family implicated in nervous system development. Proc Natl Acad Sci USA 93:9850–9857.

Van Swieten JC, Brusse E, De Graaf BM, Krieger E, Van De Graaf R, De Koning I, Maat-Kievit A, Leegwater P, Dooijes D, Oostra BA, Heutink P (2003) A mutation in the fibroblast growth factor 14 gene is associated with autosomal dominant cerebellar ataxia. Am J Hum Genet 72:191–199.

Van Wart A, Trimmer JS, Matthews G (2007) Polarized distribution of ion channels within microdomains of the axon initial segment. J Comp Neurol 500:339–352.

Verhey KJ, Meyer D, Deehan R, Blenis J, Schnapp BJ, Rapoport TA, Margolis B (2001) Cargo of kinesin identified as JIP scaffolding proteins and associated signaling molecules. J Cell Biol 152:959–970.

Wang Q, McEwen DG, Ornitz DM (2000) Subcellular and developmental expression of alternatively spliced forms of fibroblast growth factor 14. Mech Dev 90:283–287.

Wang Q, Bardgett ME, Wong M, Wozniak DF, Lou J, McNeil BD, Chen C, Nardi A, Reid DC, Yamada K, Ornitz DM (2002) Ataxia and paroxysmal dyskinesia in mice lacking axonally transported FGF14. Neuron 35:25–38.

Waters J, Schaefer A, Sakmann B (2005) Backpropagating action potentials in neurones: measurement, mechanisms and potential functions. Prog Biophys Mol Biol 87:145–170.

Wittmack EK, Rush AM, Craner MJ, Goldfarb M, Waxman SG, Dib-Hajj SD (2004) Fibroblast growth factor homologous factor 2B: association with Nav1.6 and selective colocalization at nodes of Ranvier of dorsal root axons. J Neurosci 24:6765–6775.

Wozniak DF, Xiao M, Xu L, Yamada KA, Ornitz DM (2007) Impaired spatial learning and defective theta burst induced LTP in mice lacking fibroblast growth factor 14. Neurobiol Dis 26:14–26.

Xiao M, Xu L, Laezza F, Yamada K, Feng S, Ornitz DM (2007) Impaired hippocampal synaptic transmission and plasticity in mice lacking fibroblast growth factor 14. Mol Cell Neurosci 34:366–377.